CATALYSIS

Formation of active sites on transition metals through reaction-driven migration of surface atoms

Lang Xu[1]†, Konstantinos G. Papanikolaou[1]†, Barbara A. J. Lechner[2,3], Lisa Je[1], Gabor A. Somorjai[3,4], Miquel Salmeron[3,5], Manos Mavrikakis[1]*

Adopting low-index single-crystal surfaces as models for metal nanoparticle catalysts has been questioned by the experimental findings of adsorbate-induced formation of subnanometer clusters on several single-crystal surfaces. We used density functional theory calculations to elucidate the conditions that lead to cluster formation and show how adatom formation energies enable efficient screening of the conditions required for adsorbate-induced cluster formation. We studied a combination of eight face-centered cubic transition metals and 18 common surface intermediates and identified systems relevant to catalytic reactions, such as carbon monoxide (CO) oxidation and ammonia (NH_3) oxidation. We used kinetic Monte Carlo simulations to elucidate the CO-induced cluster formation process on a copper surface. Scanning tunneling microscopy of CO on a nickel (111) surface that contains steps and dislocations points to the structure sensitivity of this phenomenon. Metal-metal bond breaking that leads to the evolution of catalyst structures under realistic reaction conditions occurs much more broadly than previously thought.

Understanding the nature of the active sites on catalytic surfaces is central to understanding and improving catalysis (*1*). Low-index metal surfaces, such as the (111), (100), and (110) facets, are commonly adopted models of supported metal catalysts, particularly in computational studies, but have limitations in describing the active site under realistic reaction conditions (*2*). For example, such simple models do not account for low coordination atoms found in point defects, atomic steps, and grain boundaries in catalyst surfaces that can play a key role in determining catalytic properties (*3*). Recent scanning tunneling microscopy (STM) studies showed that subnanometer metal clusters that expose increased numbers of low coordinated atoms can be formed in situ on low-index surfaces when molecules are adsorbed on them. Such metal clusters exhibit distinct catalytic (*4*–*11*) and electronic properties and dynamic structural fluxionality (*12*) compared with those of nanoparticles (NPs) with diameters >2 nm, and NPs can also restructure during reaction (*13*, *14*). Adsorbate-induced cluster formation hints at the dynamic nature of catalytic surfaces and suggests that the active sites that are formed under practically relevant reaction conditions can be substantially different from those in extended facets or in pristine NP models that are commonly used in mechanistic studies of thermal catalysis and electrocatalysis (*15*).

Although highly dispersed small metal clusters are generally prepared using controlled synthesis techniques (*16*, *17*), the formation of clusters on bulk crystals induced by adsorbates under realistic reactive conditions, to our knowledge, has not been explicitly included in previous studies. The main reason has been the difficulty of experimentally characterizing catalyst structures under the conditions that are encountered in industrial catalysis, which include high pressures and temperatures (*18*). Some of the systems that have been experimentally characterized at torr-level pressures exhibit adsorbate-induced cluster formation. CO-induced clustering has been reported on Cu(111) (*19*), Cu(100) (*20*), and CuCo (*21*) alloy surfaces. However, no CO-induced cluster formation was observed on Rh(111) when the surface was exposed to CO up to atmospheric pressure (*22*). Mixed results were reported for Pt. On a flat Pt(111) single crystal with few steps, no cluster formation was observed up to atmospheric CO pressure (*23*), whereas on vicinal (regularly stepped) Pt(557) and Pt(332), clustering was observed at torr-level CO exposures (*24*). Interestingly, on Pt(997), which has a vicinal surface with a terrace size ~1.5 times larger than that of Pt (557), step doubling, but no cluster formation, was observed (*25*).

These results point to a potential role of step-step interactions in the surface evolution under reactive environments. Accordingly, adsorbate-induced cluster formation depends on the identity of the metal surface as well as the adsorbate-metal interactions (*26*). Here, we developed an efficient framework for the prediction of adsorbate-induced cluster formation using energetics derived from density functional theory (DFT) calculations. We first discuss how we correlate the adsorbate-induced clustering effect to a single energetic parameter that can be easily computed. We then demonstrate how this methodology leads to predictions in agreement with experimental results, as well as its limitations. Next, we present a comprehensive database that includes eight transition metals and 18 adsorbates that are commonly involved in heterogeneous catalysis and discuss examples of catalytic systems that should be dominated by in situ adsorbate-induced active-site formation, thereby warranting a revisitation of their detailed reaction mechanisms. Subsequently, using kinetic Monte Carlo (KMC) simulations, we conduct a case study for CO-induced cluster formation on Cu(111). We conclude with STM data for CO adsorption on a Ni(111) surface that contains steps and dislocations, pointing to the rich structure sensitivity of this phenomenon.

Theoretical modeling of bare surfaces and surfaces with adsorbed CO

The adsorbate-induced cluster formation observed by Eren *et al.* (*19*) can be described as a three-step process (Fig. 1A): (i) ejection of step-edge or kink atoms leading to adatom formation on an adjacent terrace, (ii) adatom diffusion, and (iii) aggregation of adatoms to form subnanometer clusters. Because the first step of this process requires the breaking of surface metal-metal bonds, the energy cost of atom ejection must be overcome for this three-step process to proceed. We defined the adatom formation energy (E_{form}) as the descriptor for the initial screening of systems that could exhibit clustering. Our procedure to evaluate the adatom formation energy involved the use of two infinitely separated slab models (Fig. 1, B and C), where one is the source for the surface atom to be ejected and the other is the sink where the adatom lands after ejection from the first slab. Detailed definitions are provided in the supplementary materials (SM).

Here, we considered three types of possible ejection sources: (i) a kink site [modeled with the (874) slab; Fig. 1, B and C]; (ii) a regular, defect-free step edge [modeled with the (211) slab; fig. S8A]; and (iii) the (111) terrace (fig. S8B). Because E_{form} is a thermodynamic parameter, it does not fully capture the kinetics of adatom formation, which is determined by the energy barrier. Accordingly, E_{form} values calculated here can be considered as lower bounds for the activation energy barriers for adatom formation. We later demonstrate, using results on Cu(874), that the difference between E_{form} and the true activation energy barrier for atom ejection is very small (<0.02 eV). Total energies were evaluated by using periodic DFT calculations (GGA-PBE) with the Vienna ab initio simulation package (see SM for computational details).

[1]Department of Chemical and Biological Engineering, University of Wisconsin–Madison, Madison, WI 53706, USA. [2]Department of Chemistry and Catalysis Research Center, School of Natural Sciences, Technical University of Munich, 85748 Garching, Germany. [3]Division of Materials Science, Lawrence Berkeley National Laboratory, Berkeley, CA 94720, USA. [4]Department of Chemistry, University of California, Berkeley, Berkeley, CA 94720, USA. [5]Department of Materials Science and Engineering, University of California, Berkeley, Berkeley, CA 94720, USA.
*Corresponding author. Email: emavrikakis@wisc.edu
†These authors contributed equally to this work.

As a case study, we first examined the adatom formation process under vacuum (Fig. 2A) and in the presence of CO (Fig. 2B), a common reactive species in catalytic applications. In the absence of adsorbates, adatom formation on unreconstructed (111) surfaces of eight face-centered cubic (fcc) transition metals (Ag, Cu, Au, Pd, Ni, Rh, Pt, and Ir) by ejection of a (874) kink atom was always the most energetically preferred among the three aforementioned ejection sources ($E^{vac}_{form\ (111)\downarrow}^{(874)} < E^{vac}_{form\ (111)\downarrow}^{(211)} < E^{vac}_{form\ (111)\downarrow}^{(111)}$; see Fig. 2A). Further, the magnitude of the E^{vac}_{form} followed the same trend as that of the bulk cohesive energies (*27*) of the metals (pink squares in Fig. 2A). Two notable exceptions were Au and Pt, whereby despite increasing the cohesive energy (i.e., the "hardness" of a bulk metal) with respect to the previous metal in the series (Cu and Rh, respectively), the respective atom ejection energy decreased compared with that of the previous metal. This result demonstrates that the bulk metal hardness does not entirely capture atom ejection energetics.

We then investigated the effect of CO adsorption on the adatom formation from (874) kink atom ejection (Fig. 2B) at the dilute limit [one adsorbate per (874) unit cell, or 1/14 monolayer (ML) because each unit cell consists of 14 surface metal atoms; see fig. S1 for the structure of the (874) surface model]. On Ag(874), Cu(874), and Au(874) (ranked in the order of increasing bulk-metal cohesive energy), CO facilitated adatom formation ($E^{ad}_{form} < E^{vac}_{form}$), whereas on the remaining five metals studied, CO inhibited adatom formation. This mixed adsorbate effect was caused by the varying binding properties of the adsorbates across different metal surfaces (see SM for a detailed discussion).

The calculated E_{form} values on the eight metal surfaces (Fig. 2B) spanned a wide energy range from 0.42 to 2.11 eV, demonstrating the large variance in cluster formation potential across the periodic table. We expect CO to induce adatom formation from Ag(874), Cu(874), and Au(874) at near-ambient temperatures because the calculated $E^{ad}_{form\ (111)\downarrow}^{(874)}$ values (0.58, 0.68, and 0.42 eV, respectively) were below the 0.75-eV threshold, defined as the energy barrier for a room-temperature reaction with a rate constant of 1 s^{-1} (see SM) (*26*); additionally, the $E^{ad}_{form\ (111)\downarrow}^{(874)}$ values were also below the desorption barriers of CO [i.e., the absolute value of CO binding energy on the (874) surface of the corresponding metal; see table S8], indicating that CO-induced atom ejection should occur before CO desorption. On the remaining five metal surfaces, the adsorption of CO at low coverages hindered adatom formation; additionally, because the $E^{vac}_{form\ (111)\downarrow}^{(874)}$ values are well above 0.75 eV, even without the presence of CO, clustering might only occur at higher temperatures. We note that adatom formation could depend strongly on the adsorbate coverage. We later demonstrate that adatom formation from Cu(874), Ni(874), and Pt(874) occurs more readily at higher CO coverages (see SM for a detailed discussion).

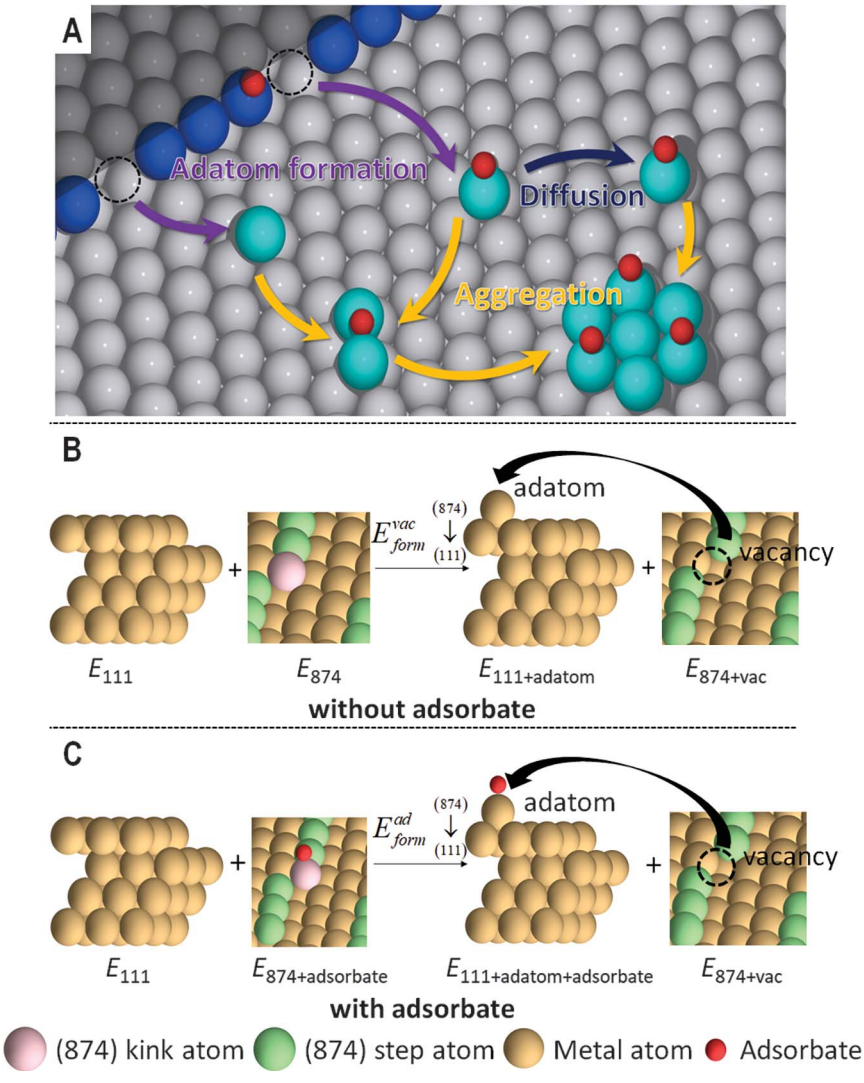

Fig. 1. Definition of adatom formation energy. (**A**) A simplified, atomic-scale illustration of the cluster formation process on a close-packed transition-metal surface due to ejection of step-edge atoms. Dashed circles indicate step-edge vacancies formed after metal atom ejection. Blue, metal atoms on a step edge; turquoise, adatoms and clusters on the terrace; gray, terrace metal atoms (the shaded area denotes the upper terrace atoms at the top-left corner); red, adsorbate species (atomic or molecular). (**B** and **C**) Schematic representations of the definitions for the adatom formation energy due to ejection of (874) kink atoms. The adatom formation energy is defined under vacuum (B) and with an adsorbate involved in the process (C) (E^{vac}_{form} and E^{ad}_{form}, respectively). All graphics represent cross-sectional views of the respective slabs used in the calculations.

Our predictions based on results shown in Fig. 2B are in agreement with ambient-temperature high-pressure (0.1 to 10 torr) STM (HP-STM) results indicating that CO could induce cluster formation on Cu(111) (*19*) but not on Rh(111) (*22*). The mixed CO-induced clustering behavior on vicinal Pt stepped surfaces [i.e., surfaces with (211)-like step-edge structures] that was observed experimentally (*24*, *25*) could be explained by taking into account the CO coverage effect on Pt steps (see SM for a detailed discussion). Specifically, a fully CO-covered step edge substantially destabilized Pt(211) step-edge atoms and facilitated atom ejection. (Note that CO coverage had a minimal effect on the energy of the final state after adatom formation.) Stress energy at steps and the vicinity of surface dislocations, as well as interactions between steps, could also considerably affect the energetics of step atom ejection (*28*). Explicit modeling of high coverage on vicinal surfaces would be suitable for a more detailed

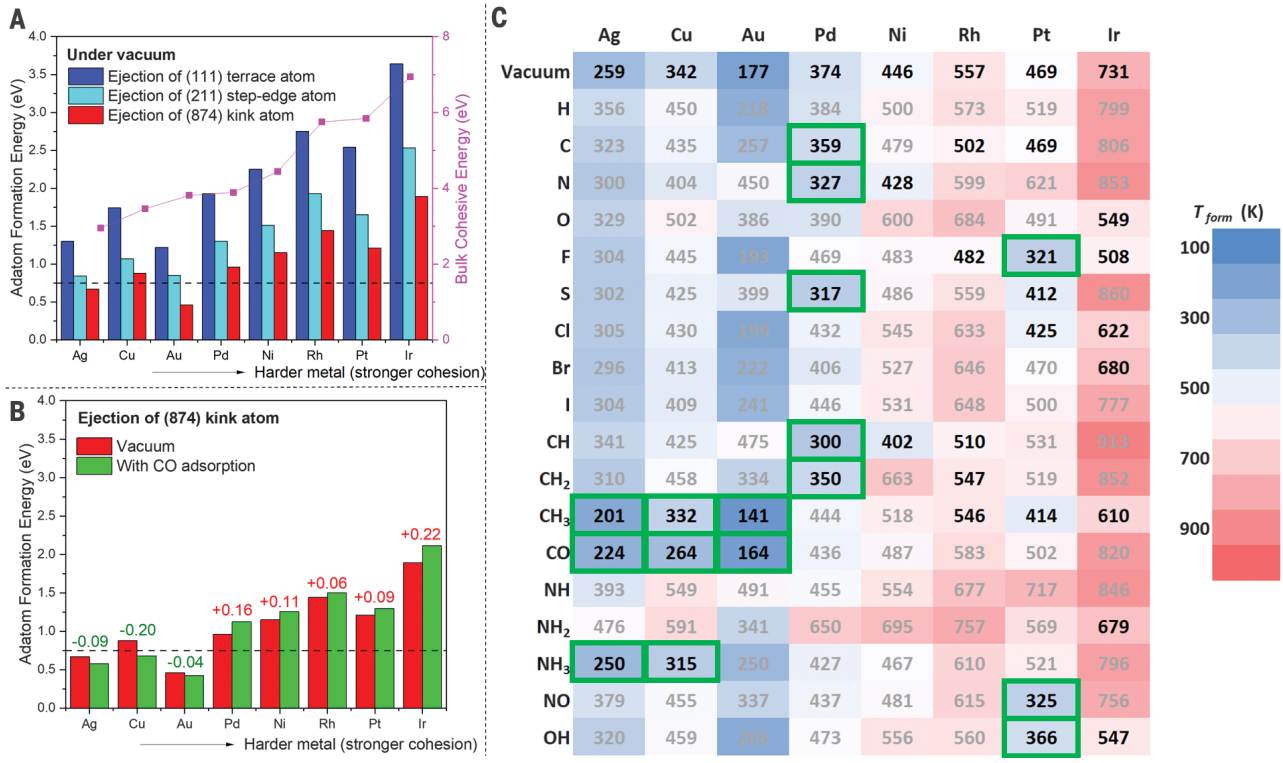

Fig. 2. Adatom formation energies and temperatures. (**A**) Comparison of calculated adatom formation energies under vacuum on the (111) facets of eight fcc transition metals by atom ejection from a (874) kink, a (211) step edge, and a (111) terrace. The experimental bulk cohesive energies from (*27*) (pink squares) are provided for comparison. (**B**) Comparison of calculated adatom formation energies on the (111) facets of fcc transition metals from the ejection of a (874) kink atom under vacuum and in the presence of CO at 1/14 ML (low-coverage limit). The numbers above the bars indicate the difference between adatom formation energy values under vacuum and in the presence of CO. In (A) and (B), the horizontal dashed line indicates the 0.75-eV threshold below which a typical surface deformation event may be expected to occur per second at ambient temperature. (**C**) Heatmap of estimated adsorbate-induced adatom formation temperatures (T^{ad}_{form}; in K) on the (111) surfaces of fcc transition metals. Except for NH_2-induced atom ejection on Au, where (111) ejection is preferred, (874) kink is the preferred atom ejection source for all the other cases. Gray-faded numbers indicate systems in which the adsorbate hinders adatom formation. Systems with both a favorable adsorbate effect for adatom formation and T^{ad}_{form} < 373 K are marked with green boxes. The eight transition metals are listed from left to right in ascending order of experimental bulk cohesive energy.

investigation of specific systems. Nonetheless, our model serves as an indicator of the tendency toward adatom and/or cluster formation and is suitable for large-scale screening purposes.

Modeling the effect of reaction intermediates on cluster formation

Next, we extended the investigation to a wide range of adsorbed reaction intermediates (H, C, N, O, F, S, Cl, Br, I, CH, CH_2, CH_3, CO, NH, NH_2, NH_3, NO, and OH) that are commonly involved in heterogeneous catalysis. An adatom formation energy database for the above eight fcc transition metals and 18 adsorbates at their low-coverage limit [1/9 ML for (111) and (211); 1/14 ML for (874)] was constructed [tables S3 to S5 for atom ejection from (111) terrace, (211) step edge, and (874) kink, respectively]. The metal adatom formation event was always endothermic regardless of the elemental nature of the adsorbate or metal and the source facet of the metal adatom. The effect of an adsorbate on adatom formation depended strongly on its binding properties (tables S6 to S9) on the corresponding metal surfaces (figs. S9 and S10; see SM for a detailed discussion).

We did not observe any generalized adsorbate effect regarding an adsorbate facilitating or inhibiting adatom formation. Except for NH_2-induced adatom formation on Au(111), where atom ejection from the (111) terrace was preferred (see SM for a discussion of adsorbate effect on adatom formation), the (874) kink was the most energetically favorable ejection source for all other cases at the low-coverage limit of the adsorbate (tables S10 and S11), as expected given the undercoordinated nature of the kink atom. The presence and fraction of kink sites on an actual catalyst surface may strongly depend on its synthesis procedure. Therefore, ejection from the other two sources (regular step and terrace) may still be relevant (see SM for a detailed discussion).

To establish a connection with realistic catalytic reaction conditions, we estimated the temperature at which these adsorbate-induced adatom formation events might occur (T^{ad}_{form}; Fig. 2C). T^{ad}_{form} is defined as the temperature at which a rate constant of 1 s^{-1} is achieved for the adatom formation event if the reaction barrier for this elementary step can be approximated by its thermochemistry (i.e., E^{ad}_{form} for the energetically preferred source of the adatom; see SM for a detailed definition). We identified systems where adsorbate-induced adatom formation might occur at near-ambient temperature based on the following two criteria: (i) the adsorbate should facilitate the adatom formation ($E^{ad}_{form} < E^{vac}_{form}$), and (ii) the estimated T^{ad}_{form} value is lower than 373 K (100°C). Sixteen adsorbate-metal systems fell into this category (table S13), which were associated with Ag, Cu, Au, Pd, and Pt. At increased temperatures, adsorbate-induced adatom formation on the other three metals (Ni, Rh, and Ir) was also possible; examples included CH/Ni (402 K), C/Rh (502 K), and O/Ir (549 K).

One notable system we identified was CO-induced adatom formation on Cu [T^{ad}_{form} = 264 K for atom ejection from Cu(874)]. The near-ambient T^{ad}_{form} value for CO/Cu, as well as the previous HP-STM evidence for cluster

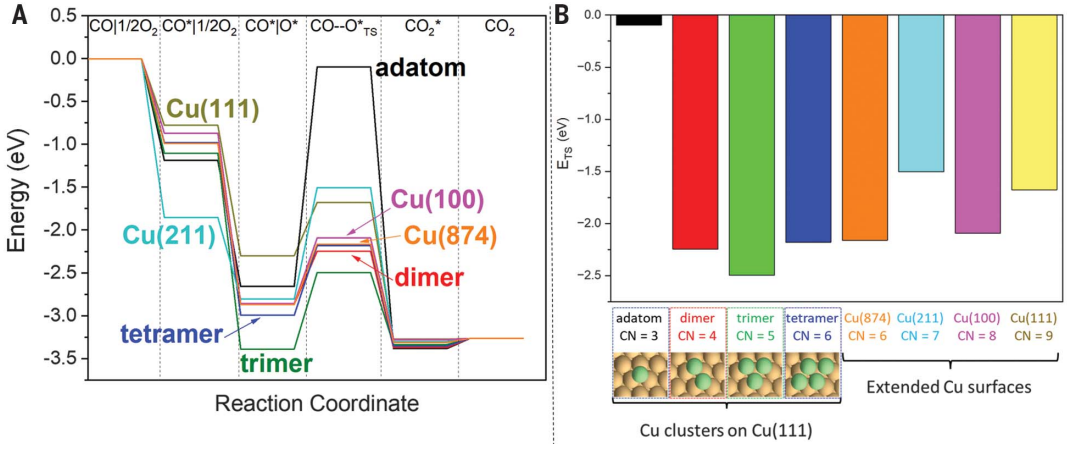

Fig. 3. Cluster effect on Cu-catalyzed CO oxidation. (**A**) Calculated potential energy diagram for CO oxidation by atomic oxygen on Cu(111)-supported Cu clusters and on pristine Cu slab models. Asterisks denote adsorbed surface species, and vertical bars denote infinite separation between adsorbed species. Zero energy is defined as the total energy of the respective clean surface plus CO and 1/2 O_2 in the gas phase. (**B**) Comparison of the calculated transition-state energy for CO--O*$_{TS}$ (E_{TS}) on Cu(111) plus adclusters and pristine Cu slab models, as compiled from data shown in (A). CN stands for the coordination number of the surface site on which the CO oxidation reaction takes place. The inset images show the atomic structures of the Cu(111) plus adcluster models. All energy values were evaluated at the low-coverage limit [1/9 ML for the (111) and (211) surfaces; 1/14 ML for the (874) surface] of each adsorbate. Green, cluster Cu atom or adatom; orange, Cu atom belonging to Cu(111).

formation on Cu(111) in the presence of CO (*19*), suggested the potential relevance of CO-induced clustering for CO oxidation on Cu catalysts. To test that hypothesis, we calculated the activation energy barrier for CO oxidation to CO_2 on Cu_n (n = 1 to 4) clusters formed on Cu(111) (Fig. 3, A and B; see SM for a detailed discussion). Among these Cu(111)-supported clusters, a Cu trimer (Cu_3) exhibited the lowest transition-state energy for CO oxidation (E_{TS}; referenced to gas-phase CO and 1/2 O_2), which was also smaller than the E_{TS} value on any extended Cu facet studied here. At room temperature, based on our DFT results, Cu_3 was estimated to be ~2×10^6 more active toward CO oxidation than Cu(874), the most active extended Cu facet. This result demonstrated the potential role of CO-induced Cu cluster sites in catalyzing CO oxidation. CO-induced clustering could also be relevant for other Cu-catalyzed industrially important catalytic reactions such as low-temperature water-gas shift (~450 to 550 K) (*29*) and methanol synthesis (~473 to 573 K) (*30*), both of which involve CO as a reactant.

Other systems with likely clustering behavior include (i) NH_3 on Ag and Cu (T^{ad}_{form} = 250 and 315 K, respectively) for ammonia oxidation (typically carried out at 383 to 553 K) (*31*); (ii) NO on Pt (T^{ad}_{form} = 325 K) for NO reduction by H_2 (~400 to 550 K); (iii) CH, CH_2, and C on Pd (T^{ad}_{form} = 300, 350, and 359 K, respectively) for methane oxidation (~673 K); and (iv) CH on Ni (T^{ad}_{form} = 402 K) and CH_3 and C on Pt (T^{ad}_{form} = 414 and 469 K, respectively) for methane steam-reforming catalysis (~973 K). If adsorbate-induced cluster formation leads to the in situ formation of the optimal cluster-type active sites for these catalytic systems, then the T^{ad}_{form} might become a limiting factor; that is, the reaction will not happen until the temperature has been raised sufficiently for adatom and active cluster-type site formation to become possible.

KMC simulations for active-site formation on Cu surfaces

To probe the kinetics of the atom ejection and cluster formation processes as a function of adsorbate coverage, we studied the CO-induced cluster formation on Cu(111) caused by the ejection of Cu atoms from Cu(874) kinks, the preferred ejection source. At different CO coverages, the activation energy barrier for kink atom ejection from Cu(874) scaled linearly with the ejection energy with a slope of near unity, thus indicating a late transition state (Fig. 4A). The ejection activation energy barrier was at most 0.02 eV larger than the respective ejection energy. Therefore, the kinetics of CO-induced atom ejection from Cu(874) was described well by its thermochemistry alone. Further, we determined that the ejection kinetics was most strongly affected by the CO coverage of the Cu(874) kink and step sites and was easiest when the kink and step sites were fully covered by CO (see SM for a detailed discussion).

We examined the overall thermochemistry associated with the formation of finite-size small clusters on Cu(111) starting from the ejection of a Cu(874) kink atom under the following three scenarios: (i) vacuum, (ii) intermediate CO coverage, and (iii) high CO coverage (Fig. 4B; see SM for a detailed definition of the cluster formation energy). As shown in Fig. 4B, the presence of CO enhanced the stability of the final clusters that formed, making the overall cluster formation process thermodynamically favorable. For intermediate CO coverage [5/14 ML on Cu(874)] corresponding to a saturated Cu step edge and kink site, the calculated adatom diffusion barrier and the activation energy barrier for adatom attachment to a preexisting Cu_5 cluster on Cu(111) to form Cu_6 (the most thermodynamically driven process for cluster size <8) were 0.04 and 0.05 eV, respectively, compared with the atom ejection barrier of 0.37 eV (Fig. 4C). At room temperature, the atom ejection should be at least five orders of magnitude slower than the diffusion and attachment processes, which confirmed that the initial adatom formation was rate limiting for the overall cluster formation process that includes atom ejection and cluster formation.

To better connect our theoretical results with experimental observations from STM, we conducted on-lattice KMC simulations facilitated by a cluster expansion to predict the energetics of nanocluster formation on Cu(111) (see SM for detailed methods) (*32*). Variation to the atom ejection energy from Cu(874) within the typical DFT error (0.2 eV) was allowed (*2*). When the ejection energy was lowered by 0.15 eV, we observed the best agreement with experimental STM measurements (Fig. 4D) at 0.3-torr CO exposure and room temperature (*19*). During a simulation period of 105.0 min, which is approximately three times the equilibration time allowed in the experiments (*19*), we observed small-sized clusters (<5 atoms) forming at early stages of the simulation. These clusters later grew to 20 to 50 atoms and were decorated with CO molecules predominantly on the peripheral sites of the clusters (Fig. 4D), similar to what was observed during the experiment (*19*). Despite the growth in cluster sizes over time, Cu_3 clusters, which are predicted to be highly active for CO oxidation (Fig. 3, A and B), were present throughout the simulation (Fig. 4D). The 0.15-eV adjustment to the ejection energy can be rationalized not only by the DFT error but also by the presence of other defects that were not accounted for in the Cu(874) surface model, which may further

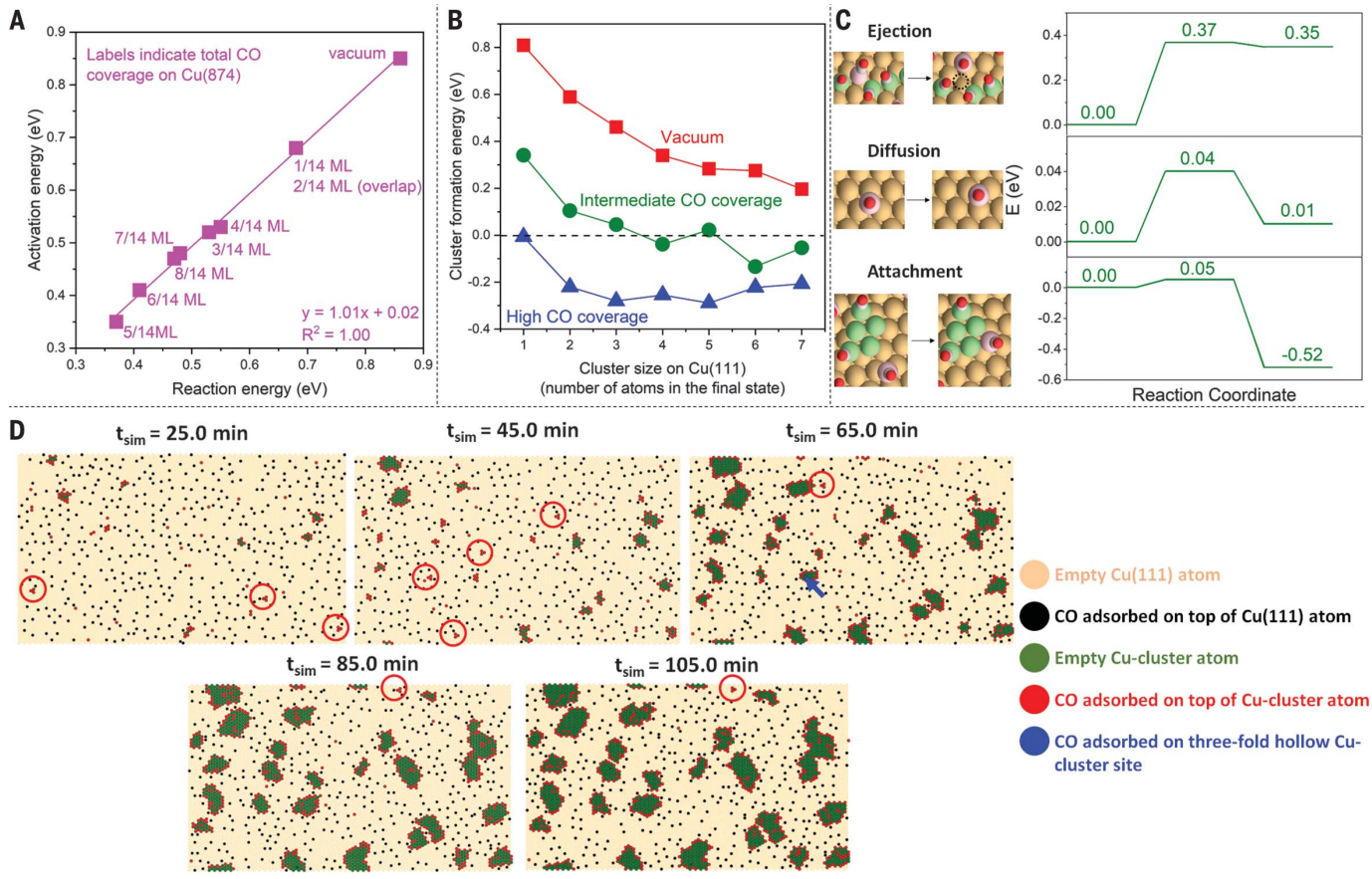

Fig. 4. CO-induced cluster formation on Cu(111) due to ejection of Cu(874) kink atoms. (**A**) Correlation between the calculated activation energy barrier and reaction energy for the kink atom ejection from Cu(874) at various CO coverages. R^2 denotes the coefficient of determination for the linear fit. (**B**) Calculated cluster formation energies (see SM for definition) due to Cu(874) kink atom ejection as a function of the Cu cluster size in the final state on Cu(111) under vacuum as well as at intermediate CO coverages [i.e., 5/14 ML CO coverage on Cu(874); half of the Cu cluster atoms formed on Cu(111) were covered by CO adsorbates] and high CO coverages (7/14 ML CO adsorbed on Cu(874); all peripheral Cu atoms and the center Cu atom of each cluster on Cu(111) were occupied by one CO molecule each]. (**C**) Potential energy diagrams for the Cu(874) kink atom ejection, Cu adatom diffusion on Cu(111), and Cu adatom addition to a Cu_5 cluster to form a Cu_6 cluster on Cu(111) at intermediate CO coverage. The minimum energy atomic structures of the initial and final states for each process are shown in the inset images. Pink, ejected Cu kink atoms; green, regular step atoms on Cu(874) and the preexisting Cu_5 cluster on Cu(111); orange, other Cu atoms; red, O; gray, C. (**D**) KMC snapshots of Cu(111) surface exposed to 0.3-torr CO at room temperature at various simulation times (t_{sim}) over a total period of 105.0 min. A fully CO-covered Cu(874) kinked step edge, with 25% of the total number of Cu(111) terrace atoms, was assumed to be implicitly present and available for atom ejection. Red circles in individual snapshots indicate Cu_3 clusters that are highly active for CO oxidation. CO adsorption at hollow sites on Cu clusters (blue circles) are very rare and indicated by the blue arrow. CO adsorbed on Cu(111) is indicated by small black circles, located in between Cu adatoms and clusters. Very many small black circles located in between Cu adatoms and/or clusters represent CO adsorbed on top of Cu(111) atoms.

facilitate local atom ejection (see discussion of the CO/Ni system in the next section).

Structure sensitivity from STM

The results in Fig. 2, A and B, point to a substantial structure sensitivity of the adatom formation, suggesting that the ejection energy decreased as the coordination number of the atom to be ejected decreased. To explore the role of defect sites and strain, we investigated the effect of CO on a Ni(111) single crystal that exhibited edge and screw dislocation defects using STM. Two types of steps, straight and undulating ones, were observed, both of atomic height (~0.2 nm). Unexpectedly, we observed that Ni adatoms and small clusters formed upon exposure to CO even at 77 K (Fig. 5). At low CO exposures, the undulating step edges became decorated by what appeared as bright protrusions, whereas straight step edges remained pristine (Fig. 5A). Several bright protrusions appeared on the terraces, exhibiting an apparent height larger than that of CO adsorbates (typically around 50 pm) and smaller than that of a full atomic step. We propose that these bright spots contain a few Ni atoms covered with CO.

Upon further CO exposure, the decoration of the undulating steps became denser and the number of clusters on the terraces increased (Fig. 5B). The streaky appearance of many clusters indicates that they were mobile under the STM tip and thus not strongly bound to the terrace sites (movie S1). As the CO exposure increased further, the straight steps also became decorated with CO molecules on every other Ni step atom (Fig. 5C). The unchanged step brightness suggests that Ni atoms were not involved in the decoration of the straight steps, in contrast to that of the undulating steps. Among some of the smallest clusters (see Fig. 5D), individual protrusions, dimer, and trimer species could be observed, which could be interpreted as one, two, and three Ni adatoms covered with CO molecules, respectively.

To better understand the formation process of the Ni adatoms and clusters, we followed the evolution of the surface during continuous exposure to ~4×10^{-9} torr CO in situ (see movie S2). Figure 5, E and F, shows derivative images (to enhance the contrast) of two frames from movie S2, which indicate that clusters were first limited to the terrace in the top

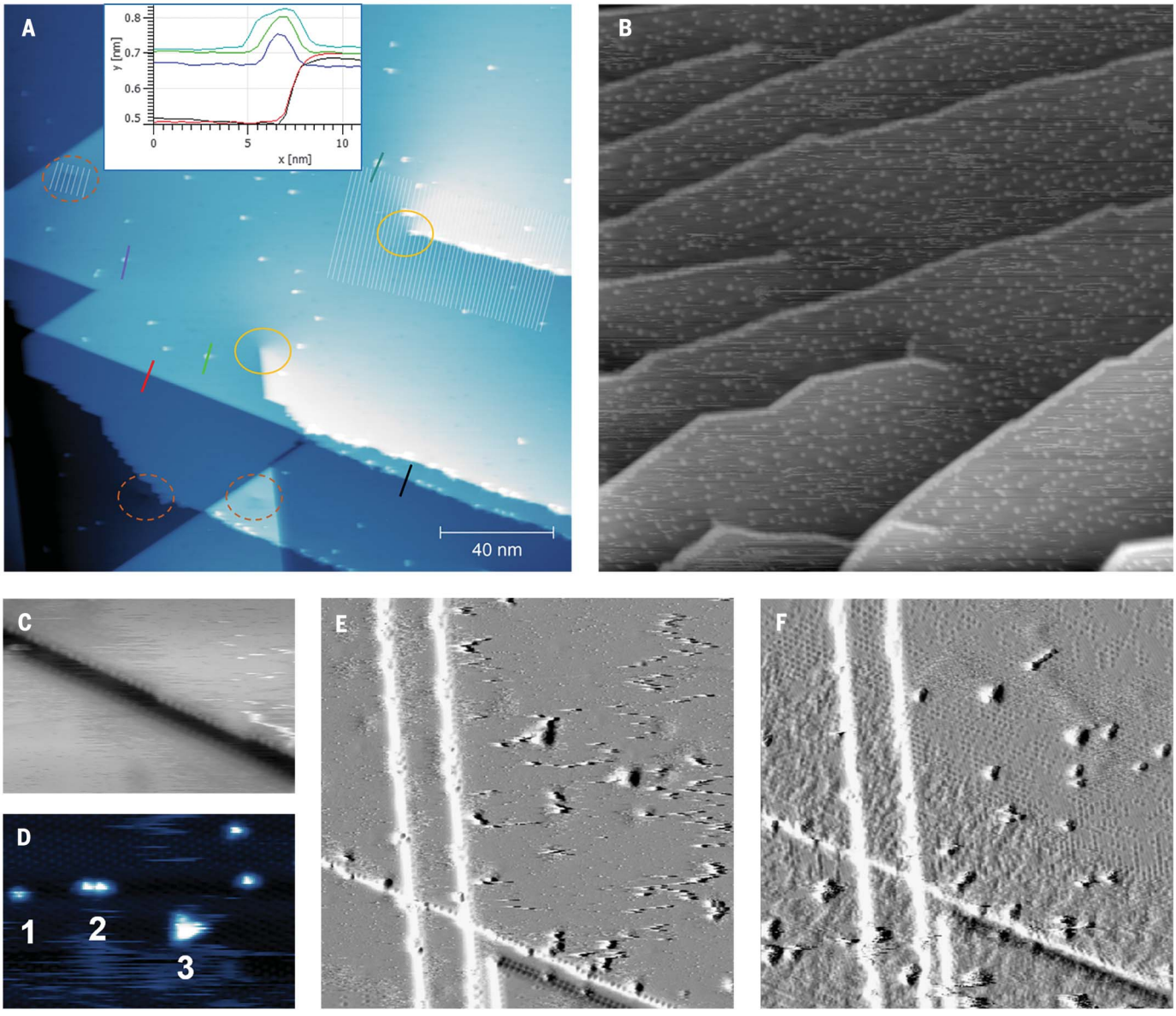

Fig. 5. STM images showing the effect of CO exposure on a defective Ni(111) surface. (**A**) At low CO exposure (background pressure of $<1 \times 10^{-10}$ torr), step-edge decoration and a few clusters on terraces are observed. Several screw and edge dislocations are present on the surface, which are indicated by yellow circles and red dashed circles, respectively. A series of line profiles across one of each type of dislocation is hinted at by semitransparent white lines, which were used to determine the change in step height (see SM). For comparison, line profiles are shown in the inset, which illustrate that straight (red) and wiggly (black) steps are of comparable height namely ~0.2 nm, and that clusters on the surface (green to blue) are of smaller heights. (**B**) Upon exposure to 3×10^{-10} torr CO for 20 s, the density of step decoration and clusters increases. Note that many clusters are mobile under the STM tip, resulting in a streaky appearance. (**C**) Upon exposure to 2×10^{-9} torr CO for 15 s, the straight steps exhibit adsorbate molecules in a p(2 × 2) arrangement, but the apparent step brightness remains the same. (**D**) Small clusters often appear as individual protrusions, dimer, and trimer species, which might be interpreted as one, two, and three Ni adatoms covered with CO molecules (recorded after extended exposure to 4×10^{-9} torr CO). (**E** and **F**) Derivative images of two frames from an STM movie recorded during exposure to ~4×10^{-9} torr CO show the progression of the interaction between CO and the defective Ni surface. Imaging parameters were as follows: temperature of 77 K [(A) to (F)]; bias voltages and tunneling currents of V_b = 100 mV and I_t = 150 pA [(A) and (C) to (F)] and V_b = 200 mV and I_t = 50 pA (B); and image sizes of 200 nm by 200 nm [(A) and (B)], 15 nm by 10 nm [(C) and (D)], and 30 nm by 30 nm [(E) and (F)].

right (Fig. 5E) but start to cover the rest of the surface after longer CO exposure (Fig. 5F). As the CO coverage increases, some clusters became locked into place by adsorbed CO molecules and appeared less streaky. An increase in apparent background roughness indicates that CO adsorption started from the step edges and then propagated into the terraces; p(2 × 2) chains along the steps and some molecules in the bottom left of Fig. 5E turn into a mostly covered bottom left half of Fig. 5F.

Based on our theoretical results (see Fig. 2C), the estimated T_{form}^{ad} value for CO-induced atom ejection from unstrained Ni(874) should be 487 K, which is well above the experimental temperature of 77 K. We propose that the large local strain near dislocations combined with a high degree of undercoordination characterizing the step defect sites could lead to a substantial decrease in the cluster formation temperature. To this end, we conducted

additional DFT calculations using a strained Ni (874) kink slab as a model for local dislocation defects (see SM for details). Our results demonstrate that the atom ejection from a kinked step site [$E^{ad}_{form\ (111)}$ = 1.26 eV for CO-induced atom ejection from the Ni(874) kink at the low-coverage limit of 1/14 ML; see table S5] would be energetically favored compared with that from a regular step [$E^{ad}_{form\ (111)}$ = 1.67 eV for CO-induced atom ejection from the Ni(211) step edge at the low-coverage limit of 1/9 ML; see table S4]. Further, combined with high CO coverage and large local compressive strain, the adatom formation energy could be markedly reduced, which potentially leads to Ni adatom formation even at 77 K. Our calculations also predict a similar strain effect for Pt because large local compressive strain would also facilitate CO-induced adatom ejection from a Pt(874) kink (fig. S19).

Discussion

We constructed a framework for the prediction of adsorbate-induced metal-metal bond breaking in solid surfaces and subsequent cluster formation on these surfaces. The insights about the nature of the active site could serve as a starting point for the screening of catalytic systems (e.g., CO oxidation, water-gas shift, and methanol synthesis on Cu, ammonia oxidation on Ag and Cu, NO reduction by H_2 on Pt, methane oxidation on Pd, and methane steam reforming on Ni) with potential adsorbate-induced clustering behavior. The rich structure sensitivity of the cluster formation process greatly adds to the complexity of this phenomena. The energetics associated with the initial adatom formation is not only affected by the structure of the atom ejection source (low-index terrace versus step versus kink) but can also vary considerably in the presence of surface defects. In the CO/Ni case, we demonstrated that compared with pristine (211) step edges, ejection from (874) kink sites could facilitate adatom formation by 0.41 eV. Strain induced by local defects such as screw dislocations could further reduce the adatom formation energy by 1 eV or more, which resulted in cluster formation at unexpectedly low temperatures. Therefore, the DFT-based predictions for reaction-driven active-site formation that are presented in this study, particularly those based on defect-free surface models, should only serve as initial guides. Given the wide range of local defect structures on metal catalyst surfaces, it is not practical to construct a universal model that accounts for all possible atom-ejection sources. Defect-rich catalysts, on which cluster formation could take place much more easily than estimated from predictions made based on defect-free surface models, should be treated with caution on a case-by-case basis.

Importantly, our results may reshape our understanding of the nature of active sites on metal NPs under catalytic reaction conditions. The low-index crystal-surface models that are widely used to calculate reaction parameters should not be taken for granted as providing the right energetic parameters; instead, nature allows for the formation of more and new types of active surface sites in reactive environments. Although the focus of our study is on the adatom formation energetics, the size of the small clusters formed by the aggregation of ejected atoms and possible sintering of those clusters would also be determined by the reactive conditions under consideration, which, in return, can alter the coverage of surface reaction intermediates under relevant temperature and pressure. This type of insight can be obtained through more in-depth investigations of specific systems, such as our KMC case-study for CO/Cu. Our approach could be easily expanded to investigate other combinations of adsorbate and catalytic surfaces—including bulk alloys (*33*), near-surface alloys (*34*, *35*), and metal oxides (*36*, *37*)—and to further explore coverage, elemental surface composition, and strain effects.

The in situ generated cluster-type active sites tend to bridge the gap between heterogeneous and homogeneous catalysis. In the latter, metal centers consisting of one or up to a few metal atoms are often responsible for catalytic transformations (*38*). Our framework should be useful for designing more accurate active-site models in theoretical studies, as well as for guiding sophisticated in situ experimental studies on the more practically relevant catalytic systems. Further, and from the catalytic active-site synthesis perspective, we suggest that we have elucidated a bottom-up approach to nanoclusters that naturally complements the top-down approach of size-selected nanocluster synthesis (*10*, *16*). We expect that this approach will have important ramifications for both thermal catalysis and electrocatalysis.

REFERENCES AND NOTES

1. J. K. Nørskov *et al*., *Chem. Soc. Rev.* **37**, 2163–2171 (2008).
2. B. W. J. Chen, L. Xu, M. Mavrikakis, *Chem. Rev.* **121**, 1007–1048 (2021).
3. W. Huang *et al*., *Science* **373**, 1518–1523 (2021).
4. Z. Xu *et al*., *Nature* **372**, 346–348 (1994).
5. C. T. Campbell, S. C. Parker, D. E. Starr, *Science* **298**, 811–814 (2002).
6. A. A. Herzing, C. J. Kiely, A. F. Carley, P. Landon, G. J. Hutchings, *Science* **321**, 1331–1335 (2008).
7. H.-G. Boyen *et al*., *Science* **297**, 1533–1536 (2002).
8. M. Turner *et al*., *Nature* **454**, 981–983 (2008).
9. A. S. Crampton *et al*., *Nat. Commun.* **7**, 10389 (2016).
10. W. E. Kaden, T. Wu, W. A. Kunkel, S. L. Anderson, *Science* **326**, 826–829 (2009).
11. K. Ding *et al*., *Science* **350**, 189–192 (2015).
12. H. Häkkinen, S. Abbet, A. Sanchez, U. Heiz, U. Landman, *Angew. Chem. Int. Ed.* **42**, 1297–1300 (2003).
13. F. F. Tao *et al*., *Nano Lett.* **16**, 5001–5009 (2016).
14. P. L. Hansen *et al*., *Science* **295**, 2053–2055 (2002).
15. V. R. Stamenkovic *et al*., *Science* **315**, 493–497 (2007).
16. S. Vajda *et al*., *Nat. Mater.* **8**, 213–216 (2009).
17. J. Jones *et al*., *Science* **353**, 150–154 (2016).
18. G. A. Somorjai, Y. Li, *Introduction to Surface Chemistry and Catalysis* (Wiley, ed. 2, 2010).
19. B. Eren *et al*., *Science* **351**, 475–478 (2016).
20. M. Roiaz *et al*., *J. Phys. Chem. C* **123**, 8112–8121 (2019).
21. B. Eren *et al*., *J. Am. Chem. Soc.* **140**, 6575–6581 (2018).
22. P. Cernota, K. Rider, H. A. Yoon, M. Salmeron, G. Somorjai, *Surf. Sci.* **445**, 249–255 (2000).
23. S. R. Longwitz *et al*., *J. Phys. Chem. B* **108**, 14497–14502 (2004).
24. F. Tao *et al*., *Science* **327**, 850–853 (2010).
25. O. Balmes, G. Prevot, X. Torrelles, E. Lundgren, S. Ferrer, *ACS Catal.* **6**, 1285–1291 (2016).
26. B. Eren, M. Salmeron, *J. Phys. Chem. C* **123**, 8171–8176 (2019).
27. C. Kittel, *Introduction to Solid State Physics* (Wiley, ed. 8, 2004).
28. B. L. M. Hendriksen *et al*., *Nat. Chem.* **2**, 730–734 (2010).
29. A. A. Gokhale, J. A. Dumesic, M. Mavrikakis, *J. Am. Chem. Soc.* **130**, 1402–1414 (2008).
30. S. Kuld *et al*., *Science* **352**, 969–974 (2016).
31. F. Wang *et al*., *ACS Catal.* **8**, 2670–2682 (2018).
32. K. G. Papanikolaou, M. T. Darby, M. Stamatakis, *ACS Catal.* **10**, 1224–1236 (2020).
33. D. Kim, J. Resasco, Y. Yu, A. M. Asiri, P. Yang, *Nat. Commun.* **5**, 4948 (2014).
34. J. Greeley, M. Mavrikakis, *Nat. Mater.* **3**, 810–815 (2004).
35. M. Lischka, C. Mosch, A. Groß, *Electrochim. Acta* **52**, 2219–2228 (2007).
36. Z. Liang, T. Li, M. Kim, A. Asthagiri, J. F. Weaver, *Science* **356**, 299–303 (2017).
37. M. Van den Bossche, H. Grönbeck, *J. Am. Chem. Soc.* **137**, 12035–12044 (2015).
38. E. Gross, G. A. Somorjai, *Top. Catal.* **57**, 812–821 (2014).

ACKNOWLEDGMENTS

Funding: The theoretical work was supported by the US Department of Energy (DOE), Office of Basic Energy Sciences, Division of Chemical Sciences, Catalysis Science Program, under grant DE-FG02-05ER15731. The experimental work was supported by the DOE, Office of Basic Energy Sciences, Division of Materials Sciences and Engineering, under contract no. DE-AC02-05CH11231, through the Structure and Dynamics of Materials Interfaces program (FWP KC31SM). B.A.J.L. acknowledges financial support from the Young Academy of the Bavarian Academy of Sciences and Humanities and Deutsche Forschungsgemeinschaft (DFG, German Research Foundation) under Germany's Excellence Strategy EXC 2089/1-390776260 during analysis of the CO on Ni(111) adsorption and diffusion. M.M. acknowledges financial support from the Miller Institute at the University of California, Berkeley, through a Visiting Miller Professorship with the Department of Chemistry. We used resources at the National Energy Research Scientific Computing Center, a DOE Office of Science User Facility that is supported by the DOE, Office of Science, under contract no. DE-AC02-05CH11231 using NERSC award BES-ERCAP0022773. Part of the computational work was carried out using supercomputing resources at the Center for Nanoscale Materials (CNM), a DOE Office of Science User Facility located at Argonne National Laboratory that is supported by DOE contract DE-AC02-06CH11357. **Author contributions:** Conceptualization: L.X., K.G.P., B.A.J.L., G.A.S., M.S., M.M.; Methodology: L.X., K.G.P., B.A.J.L., M.S., M.M.; Investigation: L.X., K.G.P., L.J., B.A.J.L.; Funding acquisition: M.M.; Supervision: M.M.; Writing – original draft: L.X., K.G.P., M.M.; Writing – review and editing: L.X., K.G.P., B.A.J.L., G.A.S., M.S., M.M. **Competing interests:** The authors declare that they have no competing interests. **Data and materials availability:** All data are available in the main text or the supplementary materials.

SUPPLEMENTARY MATERIALS

science.org/doi/10.1126/science.add0089
Materials and Methods
Supplementary Text
Figs. S1 to S28
Tables S1 to S13
References (*39*–*71*)
Movies S1 and S2
Data S1

Submitted 14 May 2022; resubmitted 21 December 2022
Accepted 14 March 2023
10.1126/science.add0089

Formation of active sites on transition metals through reaction-driven migration of surface atoms

Lang Xu, Konstantinos G. Papanikolaou, Barbara A. J. Lechner, Lisa Je, Gabor A. Somorjai, Miquel Salmeron, and Manos Mavrikakis

Science, **380** (6640), .
DOI: 10.1126/science.add0089

Mobile metal atoms underlying reactions

In heterogeneous catalysis, it is often assumed that adsorbates have minimal effects on the bonding between surface metal atoms at low temperatures and pressures. Xu *et al*. used density functional theory to find conditions in which adsorbed molecules can scavenge transition metal atoms by breaking bonds at the surface. These atoms can then form clusters, as observed in kinetic Monte Carlo simulations of carbon monoxide on copper and in scanning tunneling microscopy studies of carbon monoxide on a Ni(111) surface containing steps and dislocations. The reaction mechanisms of several catalytic systems may be dominated by in situ adsorbate-induced active site formation. —PDS

Science (ISSN) is published by the American Association for the Advancement of Science. 1200 New York Avenue NW, Washington, DC 20005. The title *Science* is a registered trademark of AAAS.